ELSEVIER

Materials Science and Engineering A261 (1999) 78–83

MATERIALS SCIENCE & ENGINEERING A

Microstructure and mechanical properties of $Mo-Mo_3Si-Mo_5SiB_2$ silicides

J.H. Schneibel *, C.T. Liu, D.S. Easton, C.A. Carmichael

Metals and Ceramics Division, Oak Ridge National Laboratory, Oak Ridge, TN 37831-6115, USA

Abstract

Molybdenum boron silicides consisting of 20–50 vol.% of α-Mo and different ratios of the intermetallic phases Mo_5SiB_2 ('T2') and Mo_3Si were prepared by arc-melting followed by dropcasting into Cu chill molds. For α-Mo volume fractions of $\approx 50\%$ sound castings were obtained. For lower α-Mo volume fractions such as 25% macroscopic cracks were often observed. Preliminary oxidation tests verified the expected increase in the oxidation resistance as the B-concentration increases and the α-Mo volume fraction decreases. Also, the formation of glass films was observed. Depending on composition and heat treatment, the room temperature flexure strengths varied usually between 300 and 600 MPa. To some extent, these variations could be rationalized by differences in the microstructures. Annealing for 1 day at 1873 K in vacuum caused distinct microstructural coarsening. Annealing was sometimes accompanied by microcracking in the Mo_3Si and the T2 phases. Cooling curves suggest that the liquidus temperature of the T2 phase is above 2400 K. Depending on the composition, final freezing of Mo–Si–B alloys was found to occur at temperatures as low as 2200 K. Care is therefore required during thermomechanical processing to avoid the formation of liquid phases. © 1999 Elsevier Science S.A. All rights reserved.

Keywords: Molybdenum; Microstructures; Glass

1. Introduction

$MoSi_2$-based refractory silicides have received substantial interest during the last 10 years because of their excellent oxidation resistance and their potential for structural applications [1]. More recently, boron-containing molybdenum silicides have been examined as well [2–11]. These intermetallic alloys do not contain $MoSi_2$, but rather α-Mo solid solution, Mo_3Si, and Mo_5SiB_2 ('T2') [6–11], or Mo_3Si, Mo_5Si_3 ('T1'), and Mo_5SiB_2 ('T2') [2–5]. Depending on the exact composition, the oxidation resistance of the alloys consisting of Mo_3Si, T1, and T2 is comparable to that of $MoSi_2$-base materials [2]. Also, these intermetallics have very high melting points, T_m. For example, T_m (Mo_3Si) = 2298 K and T_m (T1) = 2453 K. However, the fracture toughness of alloys in the Mo_3Si–T1–T2 system is likely to be low, because these alloys consists of three brittle phases. Also, the processing of such alloys is difficult [5]. The alloys consisting of α-Mo, Mo_3Si, and T2, on the other hand, are expected to have higher fracture toughnesses than the Mo_3Si–T1–T2 alloys because of the presence of α-Mo. However, their oxidation resistance will be lower, again because of the presence of α-Mo. The present paper investigates such alloys, which are easier to process and have better mechanical properties than those alloys consisting exclusively of brittle phases. Depending on composition and heat treatment, a wide range of microstructures and room temperature strengths can be obtained. Although the liquidus of the T2 phase is found to be above 2400 K, thermal arrest measurements during cooling indicate that partial liquid formation in Mo–Si–B alloys may occur at temperatures as low as 2200 K.

2. Experimental procedure

Mo–Si–B alloys were prepared by arc-melting nominally pure elements in a partial pressure (70 kPa) of argon and drop-casting into water-cooled copper molds with a diameter of 12.5 mm. For certain compositions, the viscosity of the melt was too high to allow drop casting. In these cases, elongated buttons were cast

* Corresponding author.

0921-5093/99/$ - see front matter © 1999 Elsevier Science S.A. All rights reserved.
PII: S0921-5093(98)01051-X

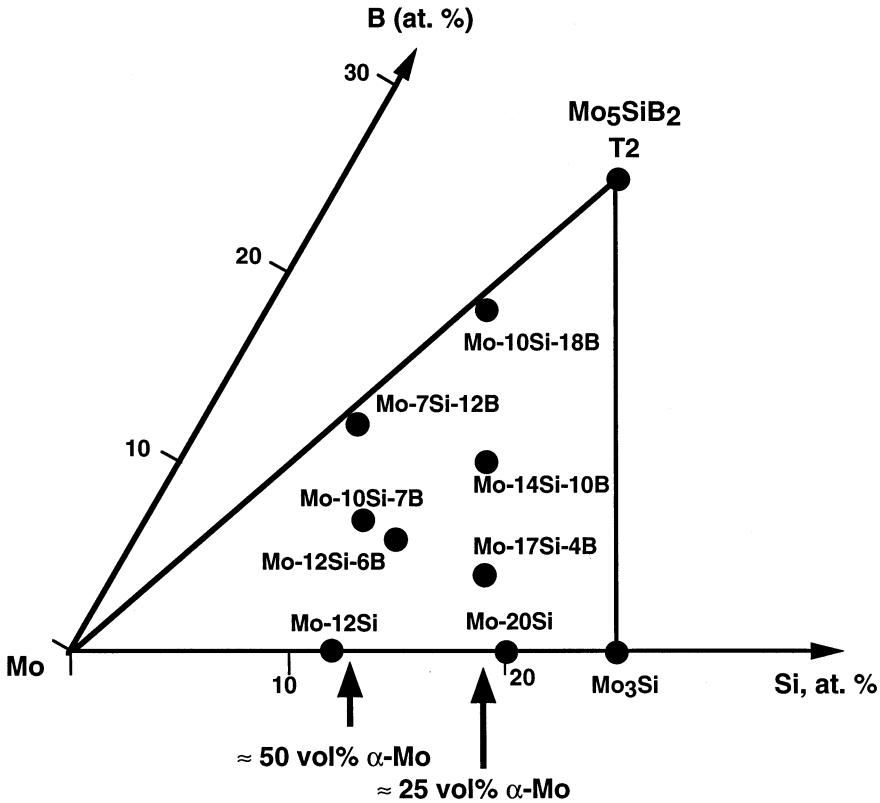

Fig. 1. Schematic ternary phase diagram summarizing the investigated compositions.

instead. The investigated compositions are summarized in the ternary phase diagram section in Fig. 1. Essentially, two sets of alloys containing ≈50 or 25 vol.% α-Mo, respectively, and different Mo_3Si to T2 ratios were prepared. Compositions are always stated in at.% in this paper. Table 1 provides estimates of the phase volume fractions. These estimates were obtained from the nominal composition and the molar volumes of pure Mo, Mo_3Si, and Mo_5SiB_2 (T2). Cast and cast and annealed specimens were polished and subsequently etched with Murakami's etch. They were examined by optical microscopy and scanning electron microscopy coupled with energy dispersive analysis (SEM/EDS). Since B could not be reliably detected by EDS, phase analysis relied on Murakami's etch attacking primarily the T2 phase [3] and on the determination of Mo:Si ratios, which are different for each of the three major phases involved. Mechanical strengths were assessed by room temperature 3-point flexure tests with a span of 20 mm. The flexure specimens had a cross section of 3 × 4 mm and prior to testing their surfaces were ground on a −325 mesh diamond wheel. Oxidation tests were carried out in uncovered Al_2O_3 crucibles in an air furnace. The oxidation rate was estimated from the surface areas and the mass losses of the specimens. Cooling curves were determined in the following way: specimens with a mass of about 4 g were placed on a

Table 1
Alloy compositions and estimated volume fractions of α-Mo, Mo_3Si, and T2 (%)

Composition (at.%)	α-Mo	Mo_3Si	T2
Mo–7Si–12B	53.1	4.1	42.8
Mo–10Si–7B	49.5	26.2	24.3
Mo–12Si–6B	43.0	36.2	20.8
Mo–12Si	49.5	50.5	
Mo–10Si–18B	28.0	4.4	67.6
Mo–14Si–10B	26.7	37.4	35.9
Mo–17Si–4B	25.8	60.3	13.9
Mo–20Si	21.1	78.9	

Table 2
Weight losses of Mo–Si–B alloys after annealing for 24 h in air, in mg/cm^2

Composition (at.%)	1473 K	1573 K
Mo–10Si–18B	25.4	33.3
Mo–14Si–10B	21.5	27.1
Mo–17Si–4B	95.5	94.2
Mo–20Si	594.5	556.2
Mo–67Si ($MoSi_2$)	≈0.1 [12]	

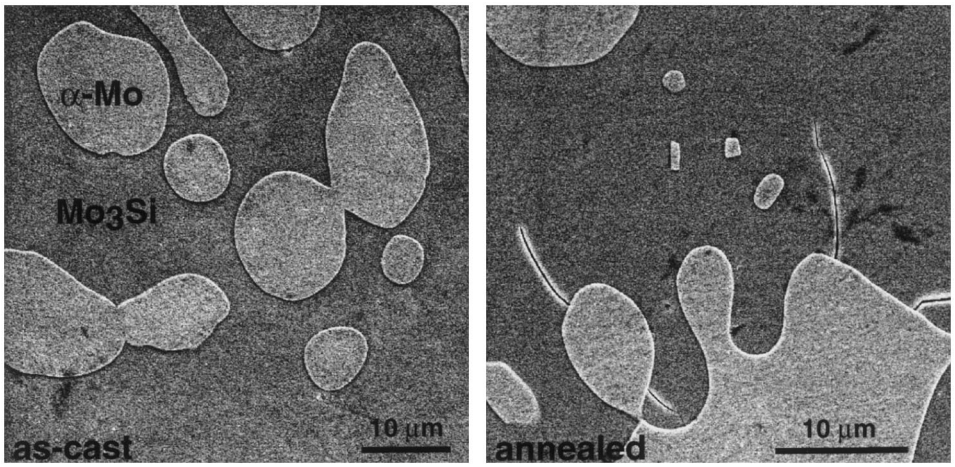

Fig. 2. SEM micrographs of polished and etched sections of as-cast and of annealed (1 day/1873 K/vacuum) Mo–20Si.

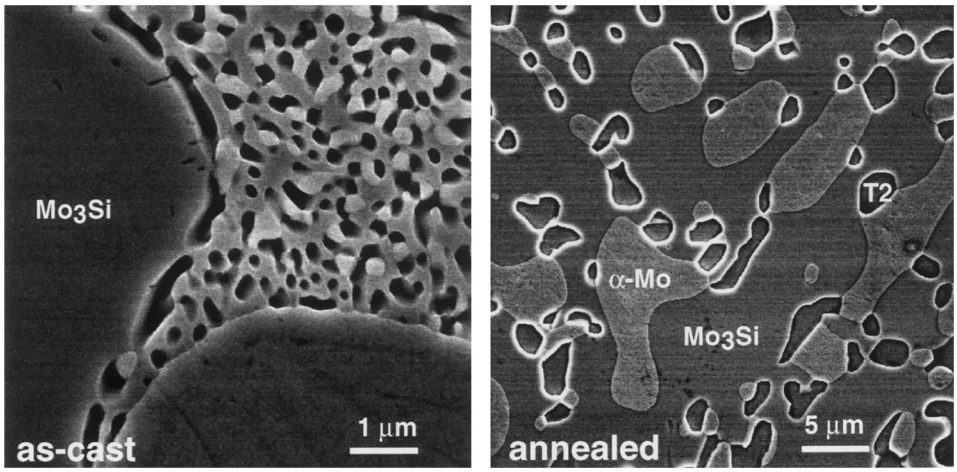

Fig. 3. SEM micrographs of polished and etched sections of as-cast and annealed (1 day/1873 K/vacuum) Mo–17Si–4B.

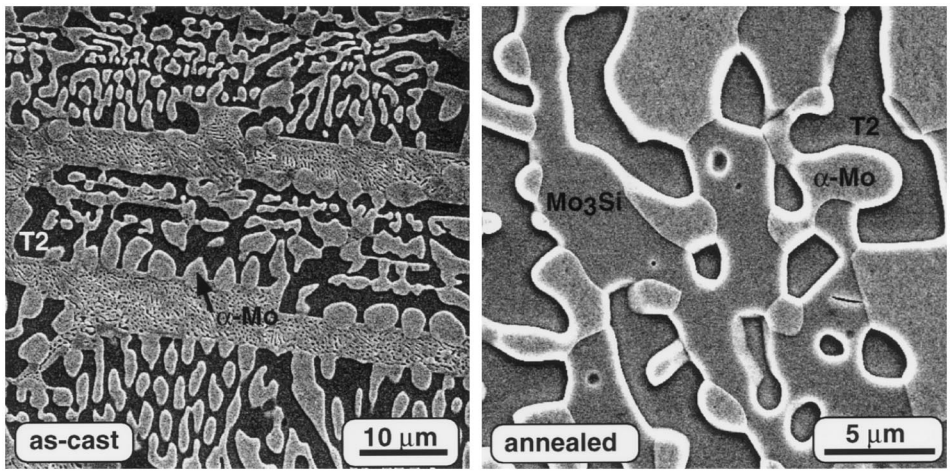

Fig. 4. SEM micrographs of polished and etched sections of as-cast and annealed (1 day/1873 K/vacuum) Mo–14Si–10B.

ZrO_2 substrate and induction-melted in a turbo-pumped vacuum. Once a specimen was completely liquid, the power setting of the induction unit was reduced and the cooling of the specimen was monitored with a 2-color pyrometer.

3. Results and discussion

3.1. Oxidation

The specimens containing ≈ 50 vol% α-Mo were

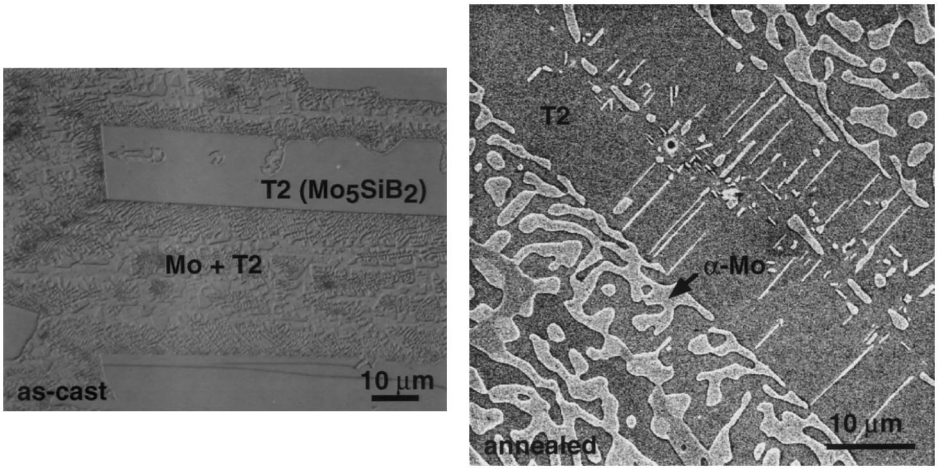

Fig. 5. Optical micrograph of polished and etched section of as-cast Mo–10Si–18B, and SEM micrograph of polished and etched section after annealing for 1 day/1873 K/vacuum.

Table 3
Room temperature flexure strengths of Mo–Mo_3Si–T2 specimens

Composition (at.%)	α-Mo volume fraction (%)	Strength (MPa, as-cast)	Standard deviation (MPa, as-cast)	Strength (MPa, 1 day/1873 K/vacuum)
Mo–7Si–12B		597	66	
Mo–10Si–7B	≈50	431	70	
Mo–12Si–6B		470	107	
Mo–12Si		322	48	
Mo–10Si–18B		303	23	604
Mo–14Si–10B	≈25	463	21	630
Mo–20Si		18		

essentially consumed after 1 day at 1473 or 1573 K in air. Therefore, Table 2 contains only oxidation data for those specimens with a volume fraction of about 25%. This data is preliminary in nature and serves only to screen the different alloys. As expected, the boron-free Mo–20Si oxidized very rapidly. After 24 h, very little was left of the original specimens. The B additions improved the oxidation resistance dramatically, although it is still well below that of $MoSi_2$ [12]. As compared to the alloy containing 10 at.% B, the alloy containing 18 at.% B oxidized slightly faster. This may be due to its slightly higher α-Mo volume fraction. Since the weight losses in Mo–Si–B alloys are particularly high at the beginning of the oxidation [2], the weight losses per unit time during further oxidation are likely to be lower than those in Table 2. After oxidation the alloys containing 10 or 18 at.% B were covered with a transparent glassy phase, which is the reason for their oxidation resistance and which gave them a 'wet' appearance.

3.2. Microstructures

The specimens with about 50 vol% α-Mo always contained particles of primary α-Mo. In Mo–20Si, which contained ≈21 vol.% α-Mo, primary α-Mo also precipitated first during solidification (Fig. 2). As solidification proceeded, a continuous Mo_3Si matrix phase formed. A vacuum anneal for 24 h at 1873 K coarsened the α-Mo particles and resulted in microcracking of the Mo_3Si matrix. Since both α-Mo and Mo_3Si have cubic crystal structures, thermal expansion anisotropy cannot be responsible for this result. Average values for the coefficients of thermal expansion over the temperature range 293–1400 K are 5.87 ppm K^{-1} for Mo and 6.03 ppm K^{-1} for Mo_3Si [13]. It is unlikely that the small difference in the expansion coefficients of the two phases (0.16 ppm K^{-1}) is responsible for the microcracking. More work is therefore needed to identify the reasons for the microcracking.

The alloy with the composition Mo–17Si–4B consisted of large primary Mo_3Si particles embedded in fine-grained 3-phase material, which consisted probably of α-Mo, Mo_3Si, and T2 (Fig. 3). Upon annealing for 1 day at 1873 K, the microstructure became much more uniform and consisted of particles of α-Mo and T2 in a Mo_3Si matrix. As compared to the Mo–20Si alloy, the annealing caused less microcracking. The anneal re-

Table 4
Comparison between measured and published melting points

	Published (K)	Measured (K)
Ni	1726	1718
Zr	2126	2113
Mo_3Si	2298	2263–2288

sulted in substantial coarsening of the microstructure (note that the magnifications of the two micrographs in Fig. three are different).

Increasing the B level, while keeping the α-Mo volume fraction close to 25% (Mo–14Si–10B) resulted in a microstructure of large T2 needles partially broken up by α-Mo (Fig. 4). The finegrained regions between the T2 needles consisted primarily of α-Mo, Mo_3Si, and T2. Annealing resulted in a fairly equiaxed microstructure. Since the Mo_3Si volume fraction in this alloy was much lower than that in Mo–17Si–4B, the Mo_3Si phase did not appear to be fully continuous. Casting of Mo–14Si–10B into an MgO mold to reduce the cooling rate resulted in a much coarser microstructure and was associated with pronounced microcracking of the T2 phase.

Fig. 5 shows the microstructure of Mo–10Si–18B, which is close to the 2-phase Mo–T2 region, and which again has a α-Mo volume fraction near 25%. This microstructure is familiar from the work of Perepezko et al. [9–11]. Long needles of the T2 phase formed as the primary phase. Upon annealing for 24 h at 1873 K, excess Mo precipitated as thin platelets in the T2 needles.

3.3. Flexure strengths

The castings containing ≈ 50 vol.% α-Mo were sound, whereas those with about 25 vol.% α-Mo always contained macrocracks. As far as possible, macrocrack-free flexure specimens were machined from the ingots. The results of the room temperature flexure strengths are presented in Table 3. For 50 vol.% α-Mo, the B free specimen, Mo–12Si, had the lowest strength. This is not surprising in view of its microstructure, which consisted of α-Mo inclusions in a brittle Mo_3Si matrix. As the B content increased, the strength increased. Qualitatively, this is due to a finer microstructure. When the α-Mo volume fraction was reduced to 25%, the strengths tended to decrease. A Mo–20Si specimen was particularly weak, presumably because it contained macrocracks. The Mo–10Si–18B specimens, which exhibited long T2 needles (Fig. 5), had an intermediate strength. The Mo–14Si–10B alloy had the highest strength. One possible reason for this is that the T2 phase was partially divided by α-Mo in the as-cast material (Fig. 4). Interestingly, the room temperature strengths increased dramatically following a 1 day anneal at 1873 K in vacuum. One factor responsible for this strength increase is the precipitation of platelike α-Mo in the T2 phase. The orientation relationship of these precipitates with the T2 phase has been determined by Sakidja et al. [11]. Qualitatively, the α-Mo platelets toughen the brittle T2 phase and divide it into smaller pieces, which results in smaller Griffith cracks and increased strength. It is also possible that the mechanical properties of the α-Mo phase itself

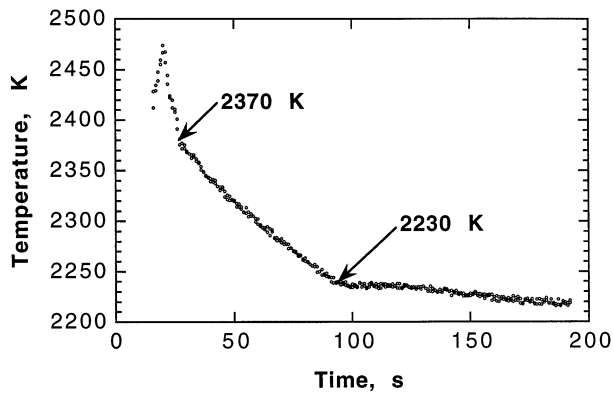

Fig. 7. Cooling curve for the T2 phase (Mo_5SiB_2).

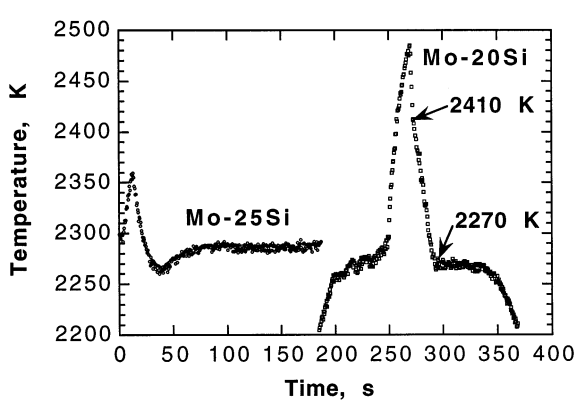

Fig. 6. Thermal arrest curves for Mo–25Si (Mo_3Si) and Mo–20Si.

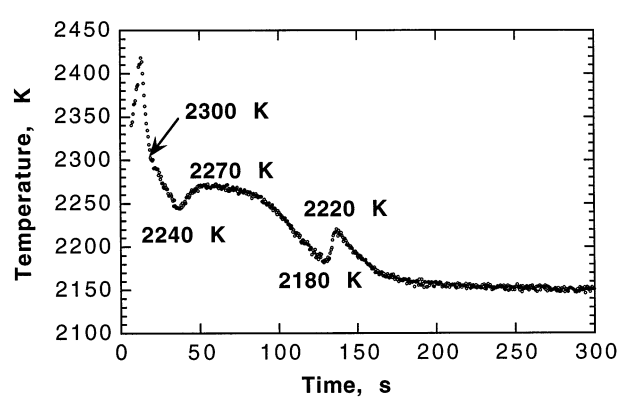

Fig. 8. Cooling curve for Mo–10Si–18B.

improve upon annealing. Distinct strength increases after annealing have also been seen in silicides with the composition Mo–12Si–8.5B [6]. For reference, the fracture toughnesses of these silicides range from 7 MPa $m^{1/2}$ in the as-cast condition to 10 MPa $m^{1/2}$ in the annealed (1 day/1873 K/vacuum) condition [6].

3.4. Melting points

Except for the respective binary systems, no melting temperature measurements are available for the ternary Mo–Si–B system. Before determining cooling curves for Mo–Si–B alloys, the melting temperatures of several known substances were measured. The results, which are summarized in Table 4 suggest that the accuracy of our melting point determinations is roughly ± 30 K. Additional complications such as undercooling due to nucleation difficulties may cause additional errors. Fig. 6 shows thermal arrest curves for Mo–25Si (Mo_3Si) and Mo–20Si. The curve for Mo_3Si shows slight undercooling followed by recalescence. The curve for Mo–20Si shows an initial change in slope as the temperature passes through 2410 K upon cooling. This indicates presumbably the formation of the primary solid phase (α-Mo). Since the cooling is quite rapid, this temperature is a lower estimate for the liquidus temperature (≈ 2520 K according to the corresponding broken line in the published phase diagram [14]). The cooling curve for stoichiometric T2 is shown in Fig. 7. In view of the metallographic analyses of Sakidja et al. [11] the change in slope at 2370 K might be related to the formation of MoB, while the change in slope at 2230 K might be related to the solidification of the last liquid. According to Sakidja et al. [11] the last liquid will solidify into Mo_3Si and T2. The cooling curve for Mo–10Si–18B (Fig. 8) is much more complicated. It shows a change in slope at 2300 K, which might be related to the formation of T2 [11]. Following this, two regions of undercooling and recalescence are observed. The second region ranges from 2180 to 2220 K. While the results obtained to date are subject to uncertainty they nevertheless suggest the presence of relatively low-melting liquids in the Mo–Si–B system. More precise knowledge of these low-melting liquids is of critical importance for the microstructure and processing of these alloys.

4. Summary and conclusions

Molybdenum boron silicides containing between 20 and 50 vol.% α-Mo were prepared by arcmelting and drop-casting. Depending on composition and heat treatment, a wide range of microstructures with widely different strengths can be obtained. Long, brittle needles of the T2 phase or the presence of a continuous Mo_3Si matrix are detrimental for the room temperature strength. Annealing may result in strength increases for various reasons such as the precipitation of α-Mo platelets in the T2 phase. For reasons which are not clear to date, annealing can also result in microcracking in the Mo_3Si or T2 phase. Alloys containing about 25 vol.% of α-Mo show some degree of oxidation resistance. Cooling curves suggest that in some compositions solidification of the last remaining liquid may occur at temperatures as low as 2200 K. This finding is of importance for the microstructural evolution and for the processing of these alloys.

Acknowledgements

This research was sponsored by the Division of Materials Sciences, US Department of Energy under contract number DE-AC05-960R22464 with Lockheed Martin Energy Research Corporation. The review of this manuscript by J.A. Horton and L.M. Pike is greatly appreciated.

References

[1] A.K. Vasudevan, J.J. Petrovic, Mater. Sci. Eng. A155 (1992) 1.
[2] A.J. Thom, M.K. Meyer, Y. Kim, M. Akinc, in: V.A. Ravi et al. (Eds.), Processing and Fabrication of Advanced Materials III, TMS, 1994, p. 413.
[3] M.K. Meyer, M.J. Kramer, M. Akinca, Intermetallics 4 (1996) 273.
[4] M. Meyer, M. Kramer, M. Akinc, Adv. Mater. 8 (1996) 85.
[5] J.H. Schneibel, C.T. Liu, L. Heatherly, M.J. Kramer, Scr. Mater. 38 (1998) 1169.
[6] J.H. Schneibel, C.T. Liu, L. Heatherly, Jr., C.A. Carmichael, in: R.R. Judkins (Ed.), Proceedings of the Twelfth Annual Conference on Fossil Energy Materials, Knoxville, TN, May 12–14, 1998.
[7] D.M. Berczik, United States Patent 5 595 616 (1997), Method for Enhancing the Oxidation Resistance of a Molybdenum Alloy, and a Method of Making a Molybdenum Alloy.
[8] D.M. Berczik, United States Patent 5 693 156 (1997), Oxidation Resistant Molybdenum Alloy.
[9] J.H. Perepezko, C.A. Nunes, S.-H. Yi, D.J. Thoma, in: C.C. Koch et al. (Eds.), MRS Symposium Proceedings Vol. 460, 1996, pp. 3–14.
[10] C.A. Nunes, R. Sakidja, J.H. Perepezko, in: M.V. Nathal et al. (Eds.), Structural Intermetallics 1997, TMS, Warrendale, PA, 1997, pp. 831–839.
[11] R. Sakidja, H. Sieber, J.H. Perepezko, in: E.S. Chen, A. Crowson (Eds.), Molybdenum and Molybdenum Alloys, San Antonio, TX, TMS, Warrendale, PA, 1998, pp. 99–110.
[12] J. Cook, A. Khan, E. Lee, R. Mapatra, Mater. Sci. Eng. A155 (1992) 183.
[13] Y.S. Touloukian (Ed.), Thermophysical Properties of High Temperature Solid Materials, vols. 1, 6, Macmillan, New York, 1967.
[14] T.B. Massalksi (Ed.), Binary Alloy Phase Diagrams, ASM, Metals Park, OH, 1986.